Scalar Control of a New Phase-Decoupling Permanent Magnet Synchronous Motor for Servo Application

Wei Cui *#, K.T. Chau *, J.Z. Jiang #, Y. Fan *, and Z. Wang *
* Department of Electrical and Electronic Engineering, The University of Hong Kong, Hong Kong, China
# Department of Automation, Shanghai University, Shanghai, China
weicui@eee.hku.hk, ktchau@eee.hku.hk, jzhjiang@yc.shu.edu.cn, yfan@eee.hku.hk, zwang@eee.hku.hk

Abstract—**This paper presents a new scalar-controlled phase-decoupling permanent magnet synchronous motor (PD-PMSM) which takes the advantages of smooth torque, fast response and good controllability for servo applications. Because of the PD nature, the proposed scalar control strategy can simply adjust the phase current amplitude and its angle with respect to the back EMF to achieve direct torque control. Experimental results are given to verify the advantages of the proposed scalar-controlled PD-PMSM.**

Keywords-PD-PMSM; scalar control; current control

I. INTRODUCTION

For high-performance servo application, the candidate electric machine needs to possess high efficiency, high power density and high controllability. In the past, dc motors were usually employed in high-performance applications for their simple controllability and good dynamic capability. However, they suffer from many drawbacks due to the use of brushes. Early attempts to replace the dc motor with brushless motor encountered the problem of cost, efficiency and controllability. With the invention of neodymium-iron-boron (Nd-Fe-B) magnets, the development of permanent magnets brushless AC (PMAC) motors has taken on an accelerated pace. Owing to high energy PMs, PMAC motors can offer higher efficiency, power factor, power density and better dynamic performance than induction motors without sacrificing reliability. Therefore, PMAC motors are playing an increasingly important role in high-performance servo applications. Those viable types of PM brushless motors are the PM synchronous motor (PMSM) [1], PM brushless DC motor (PMBDCM) [2], doubly salient PM motor (DSPM) [3], and PM hybrid motor (PMHM) [4]. Among them, the PMSM takes the definite advantage of smoother torque than its counterparts.

PMSM fed from current regulated inverters are usually used in those applications where rapid torque response and high performance operation are needed. For surface-mounted PMSM ($L_d = L_q$), the current control structure including two or three analog independent current loops is usually used in industrial scheme for its simple structure and fast dynamic response. However, as for interior PMSM (IPMSM) ($L_d > L_q$) which can offer a high-efficiency drive by utilizing the reluctance torque, an independent current loops structure is not effective for it to realize high performance operation with fast dynamic response [5], due to the presence of variable parameters and significant coupling. In that case, similar to the control of induction motor, vector control based on coordinate transformation has to be employed [6]. However, vector control needs intensive computation for coordinate transformation. Moreover, due to the high sensitivity of vector control on machine parameters, the parameter variations during operation may deteriorate the desired performance [7]. Recently, the nature of decoupling has been extended to machine design [8]. Namely, the IPMSM is designed to decouple the flux linkage between phases, so-called phase-decoupling (PD). Thus, vector control is no longer necessary.

The purpose of this paper is to present a novel scalar-controlled PD IPMSM motor drive for servo application. Based on the inherent PD nature, mutual inductance between each phase is effectively eliminated. Hence, independent current control of each phase can be accomplished. A simple scalar control of the phase current amplitude and its angle with respect to the back EMF can be devised for direct torque control. As a result, there is no need to perform the complicated coordinate transformation for vector control. Experimental results will be given to verify that the proposed scalar-controlled PD-PMSM not only offers smooth torque and fast response, but also wide constant-power operating range for servo applications.

II. MOTOR DESIGN & ANALYSIS

The schematic configuration of the proposed phase-decoupling IPMSM is shown in Fig.1, which is a 3-phase 10-pole motor. In order to improve its controllability, dynamic performance and torque smoothness to satisfy the stringent servo requirements, the proposed motor features the flux shaping air gap, the flux-focusing PM rotor, and the phase-decoupling stator windings. As the former two approaches have been generalized in our recent work [8], this paper will focus on the more details of the phase-decoupling stator windings design.

This work was supported and funded in part by the Research Grants Council of Hong Kong and the Research and Conference Grants Committee of The University of Hong Kong.

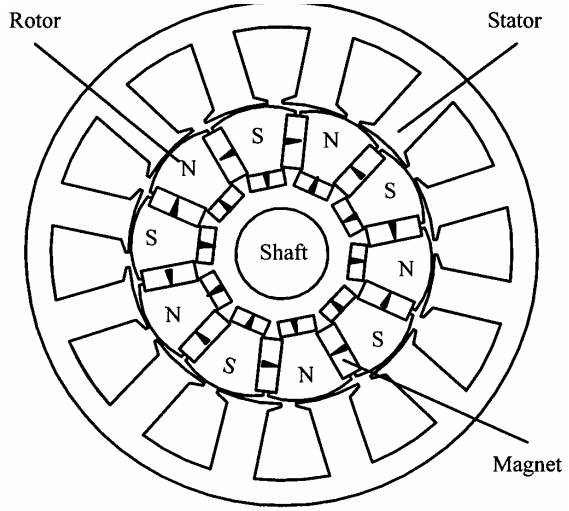

Figure 1. Proposed motor of configuration.

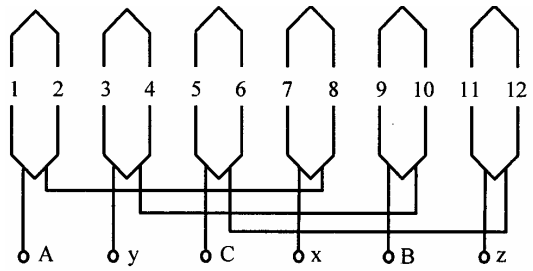

Figure 2. Stator winding connection.

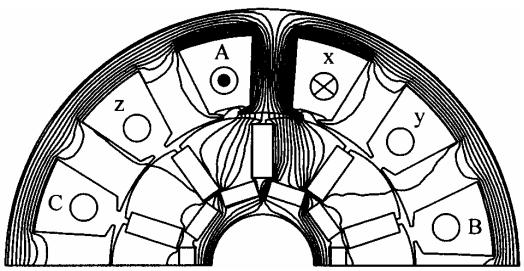

Figure 3. Static flux distribution when only phase A winding is conducted.

Differing from the conventional PMSMs, the slot number of the proposed IPMSM should be governed by (1) so as to make the flux paths of different phases symmetric.

$$Z = 2mk \tag{1}$$

where m is the motor phase number and k is an integer.

In order to minimize the cogging torque, fractional-slot winding is adopted. The slot-pole match is selected to be:

$$Z = 2p \pm 2 \tag{2}$$

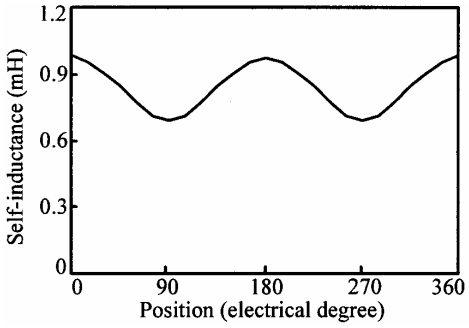

Figure 4. FEM calculated self inductance.

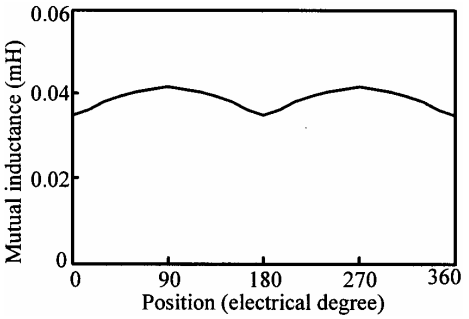

Figure 5. FEM calculated mutual inductance.

The stator of the proposed IPMSM has 12 slots. Two sides of a coil are located in two adjacent slots, for example, the slot 1 and slot 2, while another coil of the same phase is located on the opposite side of the stator, namely the slot 7 and slot 8. These two coils are connected in series. The other phase windings are arranged in the same way. The corresponding winding connection is shown in Fig.2. Due to the coil span designed to be equal to the slot pitch, the phase flux paths are independent, hence the mutual inductance of phase windings are negligible. In Fig.3, the static flux distribution in the position of 75 electrical degrees is shown when only phase A winding is conducted. The flux path of phase A is independent with very little leakage flux interacting with the windings of other two phases. The small linkage responding to the mutual inductance is mainly due to the slot flux leakage effect, which is negligible. By using the finite element method, both self inductance and mutual inductance can readily be calculated. Fig.4 and Fig.5 show the variations of self inductance and mutual inductance with respect to the rotor position. It can be found the both of them vary periodically with the rotor position in the case of iron-core saturation. However, it can be clearly seen that the self inductance is much larger than the mutual inductance. In fact, the mutual inductance is practically negligible, hence confirming the PD nature.

III. MATHEMATICAL MODEL OF PD-PMSM

As for conventional IPMSM which is described with strong decoupling and variable parameter equations as (1), vector control based on coordinate transformation has to be employed to accomplish linear decoupling control.

$$\begin{bmatrix} v_A \\ v_B \\ v_C \end{bmatrix} = \begin{bmatrix} R & 0 & 0 \\ 0 & R & 0 \\ 0 & 0 & R \end{bmatrix} \begin{bmatrix} i_A \\ i_B \\ i_C \end{bmatrix} + \frac{d}{dt} \begin{bmatrix} L_{AA} & M_{AB} & M_{AC} \\ M_{BA} & L_{BB} & M_{BC} \\ M_{CA} & M_{CB} & L_{CC} \end{bmatrix} \begin{bmatrix} i_A \\ i_B \\ i_C \end{bmatrix} + \begin{bmatrix} e_A \\ e_B \\ e_C \end{bmatrix} \tag{3}$$

where v, i, e, R, L and M are the voltages, currents, back EMFs, self inductance and mutual inductance of different phases, respectively. Because of the PD nature, the voltage equation of the proposed IPMSM is simplified to be:

$$\begin{bmatrix} v_A \\ v_B \\ v_C \end{bmatrix} = \begin{bmatrix} R & 0 & 0 \\ 0 & R & 0 \\ 0 & 0 & R \end{bmatrix} \begin{bmatrix} i_A \\ i_B \\ i_C \end{bmatrix} + \frac{d}{dt} \begin{bmatrix} L_{AA} & 0 & 0 \\ 0 & L_{BB} & 0 \\ 0 & 0 & L_{CC} \end{bmatrix} \begin{bmatrix} i_A \\ i_B \\ i_C \end{bmatrix} + \begin{bmatrix} e_A \\ e_B \\ e_C \end{bmatrix} \tag{4}$$

Since the mutual inductances are negligible, the proposed motor can not meet the preconditions for Park transformation. In the paper, the static mathematical model of the PD-PMSM based on phase is established. According to (4), the voltage equation for each phase can be further expressed:

$$v_p = R_p i_p + L_{pp} \frac{di_p}{dt} + \omega_m i_p \frac{dL_{pp}}{d\theta_m} + e_p \tag{5}$$

where $p = A$, B and C. v_p. i_p, e_p and L_{pp} stands for voltage, current, EMF and self-inductance for each phase, and ω_m, θ_m are mechanical speed and position. v_p, i_p, e_p and L_{pp} can be expressed by $v_p = V_m \sin \omega_s t$, $i_p = I_m \sin(\omega_s t - \varphi)$, $e_p = E_m \sin(\omega_s t - \delta)$ and $L_{pp} = L_{s0} + L_{s2} \cos 2\theta$ respectively, where θ is electrical position. Among these expressions, ω_s is the source frequency, φ is the phase shift between phase voltage and current and δ is the phase shift between phase voltage and EMF. V_m, I_m and E_m are the amplitude of phase voltage, current and EMF respectively, L_{s0}, L_{s2} are the primary and the 2nd-order harmonic amplitude of the self inductance. The middle two terms of (5) can be further expressed as:

$$\begin{aligned} & L_{pp} \frac{di_p}{dt} + \omega_m i_p \frac{dL_{pp}}{d\theta_m} \\ & = \omega_s I_m L_{s0} \cos(\omega_s t - \varphi) - \frac{1}{2} L_{ss} \omega_s I_m \cos(\omega_s t - 2\delta) \\ & + \frac{3}{2} \omega_s I_m L_{s2} \cos(3\omega_s t - 2\delta) \end{aligned} \tag{6}$$

The third term on the left side of (6) is generated due to 2nd-order harmonic component of the self inductance. Fortunately, this term whose frequency is the triple of primary frequency will not induce current in the motor drive without neural line. It can be regarded as the load-side neural point voltage. Hence, the phase voltage equation of the PD-PMSM can be reduced to:

$$\begin{aligned} v_p &= R_p I_m \sin(\omega_s t - \varphi) + X_0 I_m \cos(\omega_s t - \varphi) \\ &- \frac{1}{2} X_2 I_m \cos(\omega_s t + \varphi - 2\delta) + E_m \sin(\omega_s t - \delta) \end{aligned} \tag{7}$$

where $X_0 = \omega_s L_{s0}$, $X_2 = \omega_s L_{s2}$.

Using the phasor representations of i_p and v_p and substituting them in Equation (4), hence equation (8) below can be obtained:

$$\begin{aligned} V_p &= R_p I_p + (X_0 e^{j\frac{\pi}{2}} - \frac{1}{2} X_2 e^{j(\frac{\pi}{2} + 2\gamma)}) I_p + E_p \\ &= R_p I_p + j X_\beta I_p + \frac{1}{2} X_2 \sin 2\gamma I_p + j X_2 \sin^2 \gamma I_p + E_p \end{aligned} \tag{8}$$

where $X_\beta = X_0 - 0.5 X_2$, $\gamma = \varphi - \delta$.

Therefore, the whole relations between voltage, current and back EMF for each phase can be plotted on a complex plane as shown in Fig.6. Rearranging equation (5), the equation (9) below can be obtained:

$$\begin{bmatrix} V_r \\ V_a \end{bmatrix} = \begin{bmatrix} R & 0 \\ 0 & R \end{bmatrix} \begin{bmatrix} I_r \\ I_a \end{bmatrix} + \begin{bmatrix} 0 & X_a \\ -X_r & 0 \end{bmatrix} \begin{bmatrix} I_r \\ I_a \end{bmatrix} + \begin{bmatrix} 0 \\ E_p \end{bmatrix} \tag{9}$$

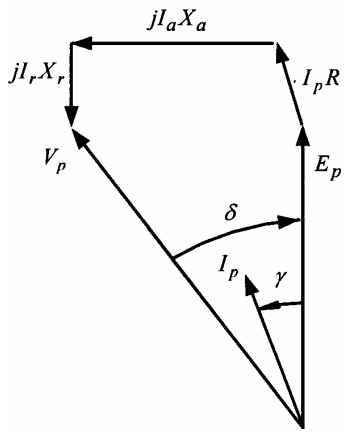

Figure 6. Scalar control operation.

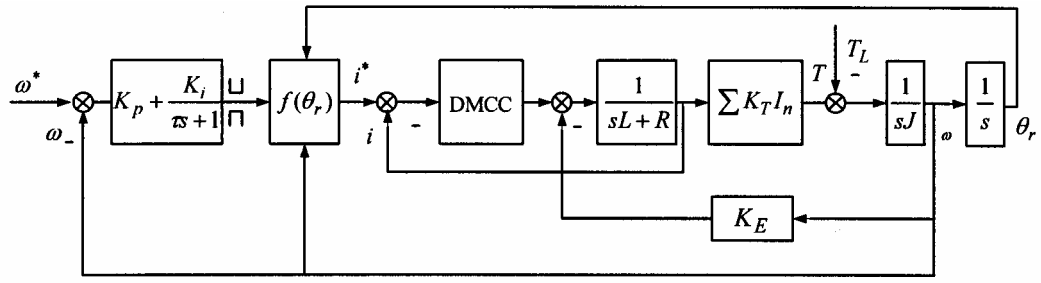

Figure 7. Schematic of scalar control system.

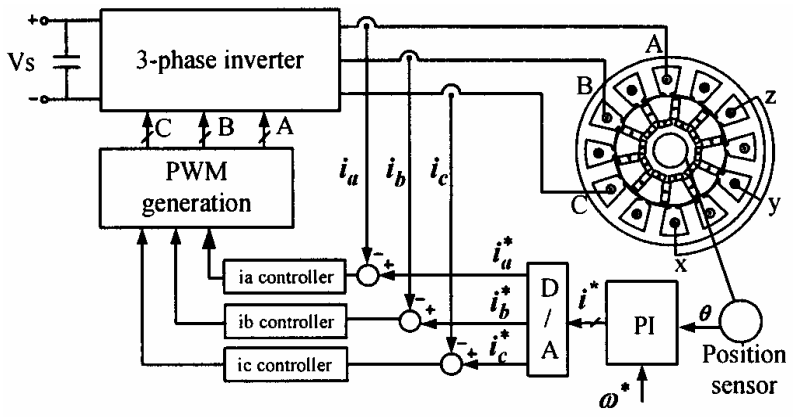

Figure 8. Block diagram of the proposed IPMSM drive system.

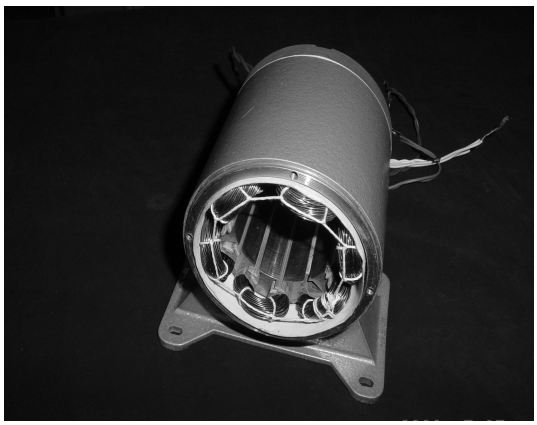

Figure 9. Stator of the proposed IPMSM.

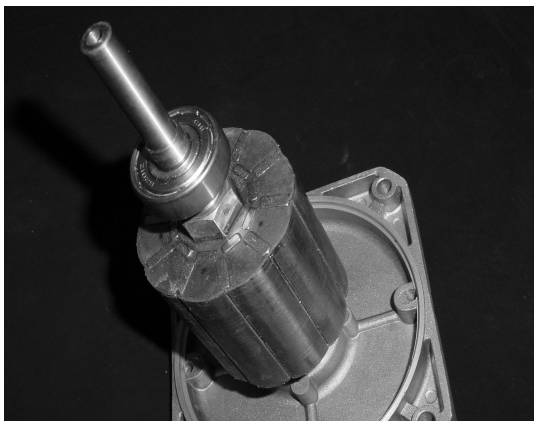

Figure 10. Rotor of the proposed IPMSM.

where V_a, I_a and V_r, I_r are active and reactive component of V_p, I_p, and $X_a = X_0 - 0.5X_2$, $X_r = X_0 + 0.5X_2$.

Based on (8), active and passive power for each phase can be expressed as:

$$P_p = U_p I_p \cos\varphi = R_p I_p^2 + E_p I_p \cos\gamma + \frac{1}{2} X_2 I_p^2 \sin 2\gamma \quad (10)$$

$$Q_p = U_p I_p \sin\varphi = X_\beta I_p^2 + X_2 \sin^2\gamma \cdot I_p^2 + E_p I_p \sin\gamma \quad (11)$$

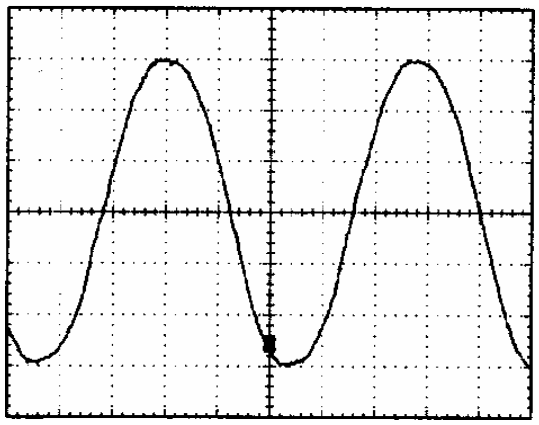

Figure 11. Experimental EMF at rated speed (5V/div, 2.5ms/div).

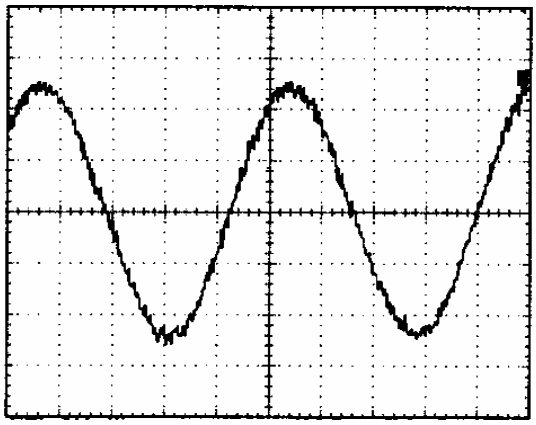

Figure 13. Experimental current at rated condition (5.5A/div, 2.5ms/div).

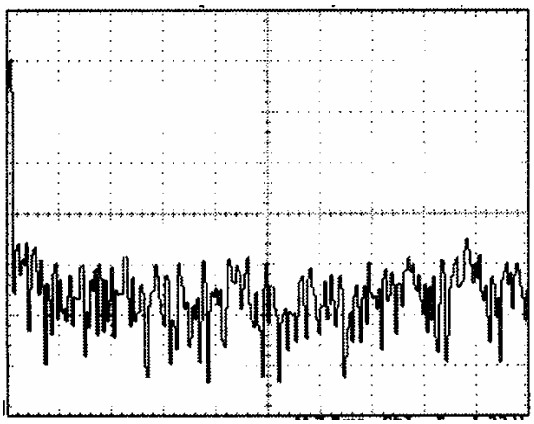

Figure 12. Harmonic spectrum of the experimental EMF (10dB/div, 500Hz/div).

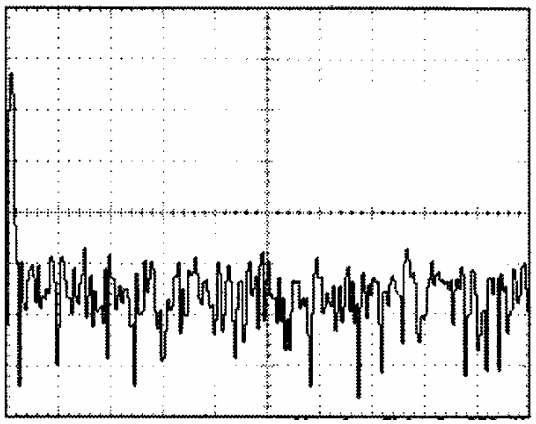

Figure 14. Harmonic spectrum of experimental current (10dB/div, 500Hz /div).

According to (10), the torque equation for each phase can be easily expressed as:

$$T_e = \frac{p}{\omega_s}(E_p I_p \cos\gamma + \frac{1}{2} X_2 I_p^2 \sin 2\gamma) \qquad (12)$$

where p is the number of pole-pairs, γ is the phase shift between E_p and I_p.

Equation (7) and (12) make up the mathematical model for PD-PMSM.

IV. PRINCIPAL OF SCALAR-CONTROL

Because of the PD nature, the proposed IPMSM presents different operation principal from conventional PMSMs. Its spatial magnetic-field is no longer circumrotating. Actually, it is a combination of three independent sinusoidally vibrating magnetic fields. Each single-phase magnetic field interacts with permanent magnetic field and produces the single-phase sinusoidally vibrating torque independently as seen in (12). Thus, the proposed IPMSM can be treated as a special structure with three single-phase motors, while the output torque can be regarded as the sum of the torque of the three motors.

As it can be seen as in (4) and (7), the motor can be described by three independent equations, which offers a definite advantage that the current of each phase can be independently controlled. Although the problem of the variable parameters and non-linearity still exist, they can be easily overcome by high-speed current-regulation techniques. Hence, a simple scalar control of phase current amplitude and its angle with respect to the back EMF can be devised for direct torque control. Complex coordinate transformation and computation are no longer necessary. Fig.6 illustrates how to control the phase current and hence the torque. In the region of constant torque operation the current is controlled in the same phase with rotational EMF for each motor phase as shown in Fig.6. The output torque can be simply controlled by adjusting the amplitude of the current with γ=0. At this time, the output torque of the PD-PMSM can be expressed as:

$$T_e = \frac{3p}{\omega_s} E_p I_p \qquad (13)$$

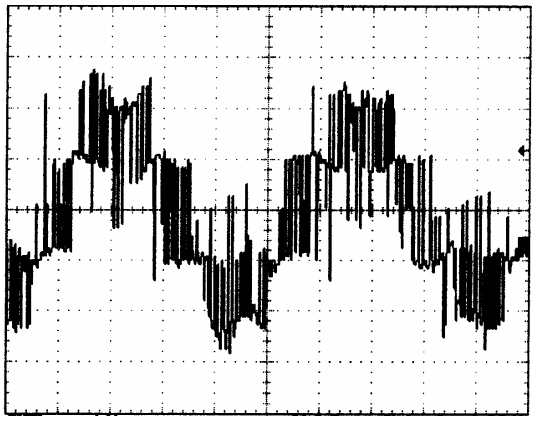

Figure 15. Measured phase voltage at rated condition (10V/div, 2.5ms/div).

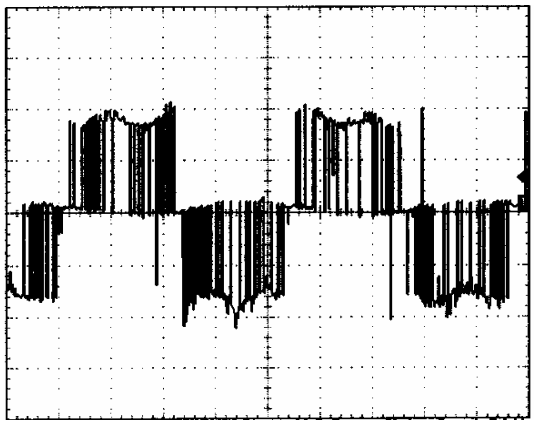

Figure 16. Measured line voltage at rated condition (20V/div, 2.5ms/div).

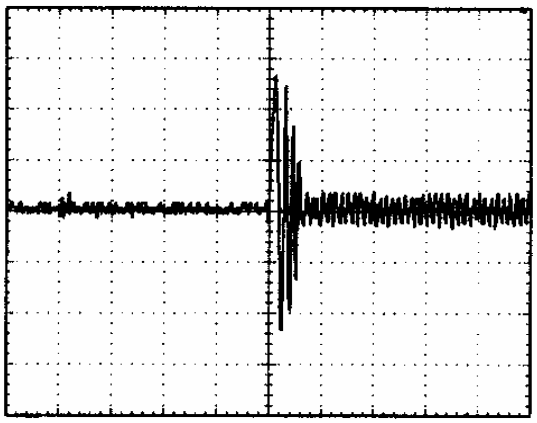

Figure 17. Measured current response at starting (5.5A/div, 100ms/div).

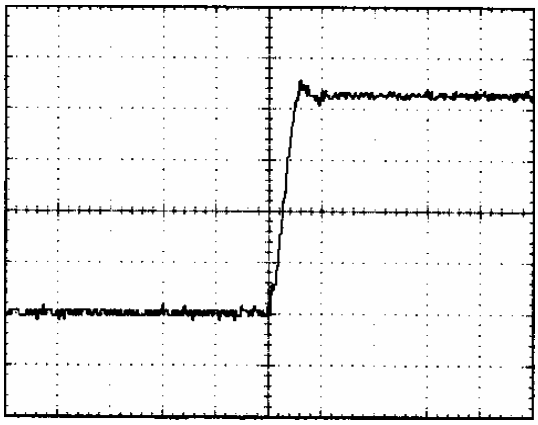

Figure 18. Measured speed response at starting (240rpm/div, 100ms/div).

If high-speed operation above the rated speed is needed, advanced conduction technique can be employed with $\gamma \neq 0$ so that phase current conducts when the rotational EMF is still negative. By employing reactive voltage $I_r X_r$ produced by the component of phase current I_r and source voltage to oppose the EMF as shown in Fig.6, thus constant power operation can be accomplished and maintained in high-speed region. Due to the contribution by the reluctance torque, the output torque can be expressed as:

$$T_e = \frac{3p}{\omega_s}(E_p I_p \cos\gamma + X_2 I_p^2 \sin 2\gamma) \qquad (14)$$

V. CONTROL STSTEM & IMPLEMENTATION

Based on a low-cost microprocessor, a dual closed-loop speed and current feedback control system is developed for the proposed PD-PMSM. As compared with the vector control of conventional IPMSM, the control is much simpler because there is no vector transformation. Fig.7 shows the block diagram of the control system, and the control process can be explained by Fig.8.

When the speed reference ω^* is set, the motor begins starting and the speed feedback is increasing gradually. The difference between ω^* and speed feedback ω is inputted into the speed proportional-integral regulator, where K_p, K_i and τ are the corresponding proportional constant and time constant. The amplified output i^* serves as an amplitude reference of phase current for the inner current control loops.

In order to produce the sinusoidal current commands and control the phase current finely, the high-resolution rotor position information θ_r is sensed from an optical encoder fixed on the motor axis. The amplitude reference i^* and rotor position θ_r are transformed to the sinusoidal current commands i_a^*, i_b^*, i_c^* through the read-only memory tables. Then, they are output through multiplying D/A converters. The phase current feedbacks are compared with i_a, i_b, i_c respectively and their differences are inputted into the current controllers. The current regulated inverter drives the phase-decoupling IPMSM so that the instantaneous phase currents can follow their reference values well.

The three independent current controllers are the key of scalar control system. The steady and dynamic performances of

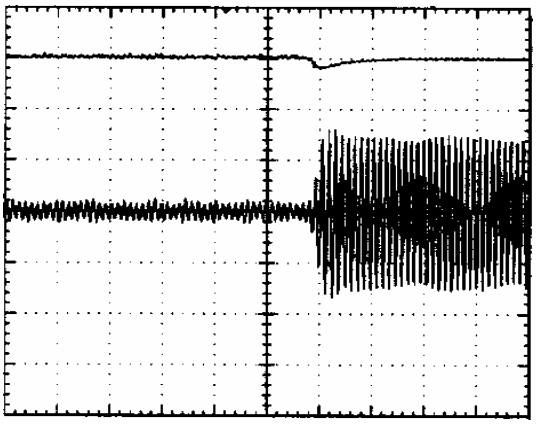

Figure 19. Measured speed (upper trace) and current (lower trace) response at sudden change of load at 700 rpm (240 rpm/div, 10A/div, 100ms/div).

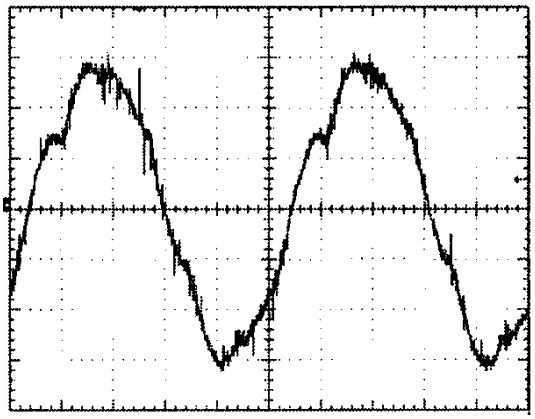

Figure 20. Experimental current at constant-power operation (5.5A/div, 1ms/div).

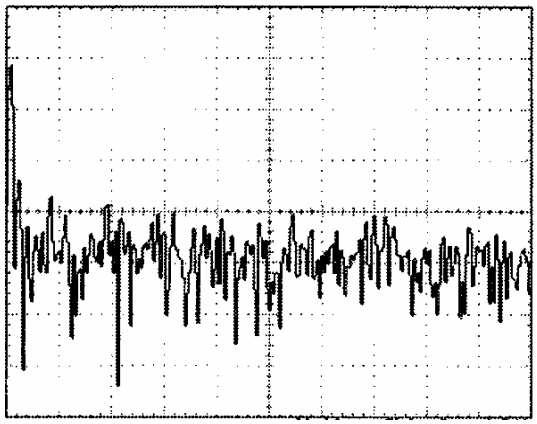

Figure 21. Harmonic spectrum of experimental current at constant-power operation (10dB/div, 1.25kHz/div).

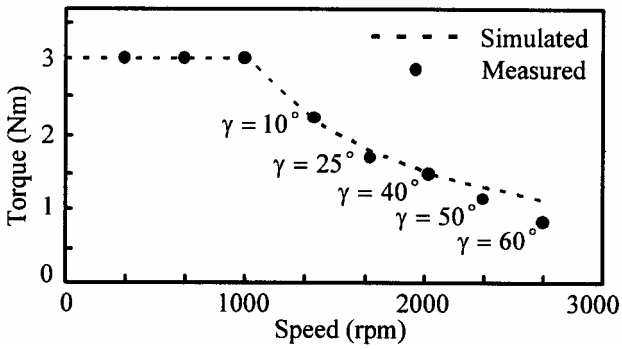

Figure 22. Comparison of simulated and measured torque-speed capabilities.

the current controllers directly determine the performance of motor output torque. Three high-performanced delta-modulated current controllers (DMCC) for each phase have been developed. The DMCC is basically a non-linear system containing sampler, zero-order holder and ideal relay units. The current command is compared with the current feedback at any moment, but the comparison result is sampled only at the interval of every control cycle. Based on the sample results, DMCC controls the on/off state of the responding switches on the phase leg so that the phase current can trace the reference signal [9]. Thus, DMCC can overcome the disadvantage of unstable switching frequency existing in most conventional hysteresis current controllers. In order to improve the dynamic response of the current regulator, the DMCC is realized with analogue circuits. The fast MOSFET inverter can works at the maximum switching frequency up to 40kHz, ensuring an excellent current control performance with minimum harmonic contents.

VI. EXPERIMENT RESULTS

Based on the newly design PD-PMSM (see Fig.9, 10 and Table I) and the proposed scalar control strategy, the whole system is prototyped for experimental verification. Fig. 11, 13 and Fig. 12, 14 show the measured waveforms and harmonic spectra of the EMF and current, respectively. It can be found that they are very sinusoidal, hence confirming the torque smoothness. Fig. 15, 16 show the measured phase and line voltage. Moreover, Fig.17 and 18 show the measured speed and current responses at starting and sudden load change, respectively. It can be seen that the rise-up time is very short with minimum overshot during starting, while the speed regulation is very good with minimum undershoot during sudden load change, hence verifying the fast response and good controllability. Fig.20, 21 illustrate the measured current and its harmonic spectra at the constant power operation with $\gamma = 50^{\circ}$. Finally, the simulated and measured torque-speed capabilities are shown in Fig.22, which confirms that the scalar-controlled PD-PMSM offers a wide range of constant-power operation. The agreement confirms that the proposed motor can offer constant torque operation at the rated torque of 3Nm and constant-power operation up to 2600rpm. There are some discrepancies at speeds beyond 2300rpm, which are mainly due to the increasing significance of nonlinear windage and frictional torques at high speeds.

VII. CONCLUSION

This paper presents and implements a new PD-PMSM motor drive for servo application. Based on the PD nature of the proposed IPMSM, a novel scalar torque control strategy has been put forward, which enables the control system to exempt from coordinate transformation for vector control. A digital speed controller based on low-cost DSP combined with high-performance current controller has been developed to operate the prototype motor drive. The results show that the proposed scalar-controlled PD-PMSM not only offers smooth torque and fast response, but also wide constant-power operating range for servo applications.

REFERENCES

[1] C.C. Chan and K.T. Chau, "An advanced permanent magnet motor drive system for battery-powered electric vehicles," IEEE Trans. Veh. Tech., Vol.45, No.1, 1996, pp.180-188.

[2] J. Gan, K.T. Chau, C.C. Chan and J.Z. Jiang, "A new surface-inset, permanent-magnet, brushless DC motor drive for electric vehicles," IEEE Trans. Magnetics, Vol.36, No.5, 2000, pp.3810-3818.

[3] M. Cheng, K.T. Chau and C.C. Chan, "Design and analysis of a new doubly salient permanent magnet motor," IEEE Trans. Magnetics, Vol.37, No.4, pp.3012-3020 (2001).

[4] K.T. Chau, J.Z. Jiang and Y. Wang, "A novel stator doubly fed doubly salient permanent magnet brushless machine," IEEE Trans.Magnetics, Vol.39, No.5, 2003, pp.3001-3003.

[5] G. Champenois, P. Mollard and J.P. Rognon, "Effective digital torque control systems for permanent magnets Converter Fed Sinusoidal Synchronous Machines," IECON 88, Singapore, 1988, pp.259-265.

[6] T.M. Jahns, G.B. Kliman and T.W. Neumann, "Interior permanent magnet synchronous motors for adjustable speed drive," IEEE Trans. Ind. Appl., Vol.22, No.4, 1986, pp.738-747.

[7] M.N. Uddin, M.A. Abido and M.A. Rahman, "Development and implementation of a hybrid intelligent controller for interior permanent magnet synchronous motor drives," IEEE Trans. Ind. Appl., Vol.40, No.1, 2004, pp. 68-76.

[8] W. Cui, K.T. Chau, J.Z. Jiang and Y. Fan, "Design of a novel phase-decoupling permanent magnet brushless ac motor," Magnetism and Magnetic Material Annual Conference, 2004, Paper No. GQ-20.

[9] P.D. Ziogas, "The delta modulation technique in static PWM inverters," IEEE Trans. Ind. Appl. , 1981, IA-17, pp.199-204.

TABLE I. MOTOR SPECIFICATIONS.

Parameters	Data
Rated voltage	40 V
Rated torque	3 Nm
Rated current	10 A
Rated speed	1000 rpm
Stator	
No. of phases	3
Outside diameter	100 mm
Inside diameter	59.6 mm
Axial length	60 mm
No. of slots	12
Winding type	Single layer
No. of coils	6
Conductor size	8×0.78mm
Coil length per phase	7812cm
Resistance per phase	0.078 Ω
Average self inductance per phase	0.93 mH
Average mutual inductance per phase	0.037 mH
Rotor	
No. of poles	12
Outside diameter	58.9 mm
Inside diameter	18 mm
Main pole magnet material	NdFeB
Main pole magnet dimensions	10.5 mm×4mm×60mm
Auxiliary pole magnet material	NdFeB
Auxiliary pole magnet dimensions	7.2 mm×3mm×60mm
Magnet remanence	1.1T
Magnet coercive	676kA/m